

2D topological matter from a boundary Green's functions perspective: Faddeev-LeVerrier algorithm implementation

Miguel Alvarado^{1*} and Alfredo Levy Yeyati¹

¹ Departamento de Física Teórica de la Materia Condensada C-V, Condensed Matter Physics Center (IFIMAC) and Instituto Nicolás Cabrera, Universidad Autónoma de Madrid, E-28049 Madrid, Spain

* miguel.alvarado@uam.es

March 9, 2022

1 Abstract

2 Since the breakthrough of twistrionics a plethora of topological phenomena in correlated
3 systems has appeared. These devices can be typically analyzed in terms of lattice mod-
4 els using Green's function techniques. In this work we introduce a general method to
5 obtain the boundary Green's function of such models taking advantage of the numer-
6 ical Faddeev-LeVerrier algorithm to circumvent some analytical constraints of previous
7 works. We illustrate our formalism analyzing the edge features of a Chern insulator, the
8 Kitaev square lattice model for a topological superconductor and the Checkerboard lat-
9 tice hosting topological flat bands. The efficiency and accuracy of the method is demon-
10 strated by comparison to recursive Green's function calculations.

11

12 Contents

13	1 Introduction	2
14	2 bGF method for 2D lattice models	4
15	3 Faddeev-LeVerrier algorithm	6
16	4 Tight-binding models	7
17	4.1 Chern insulator	7
18	4.2 2D Kitaev square lattice	9
19	4.3 Flat band Checkerboard lattice	11
20	5 Comparison with recursive approaches	12
21	6 Conclusions and outlook	14
22	A Exact Hamiltonian diagonalization	15
23	B Faddeev-LeVerrier algorithm	15
24	References	17

25

26

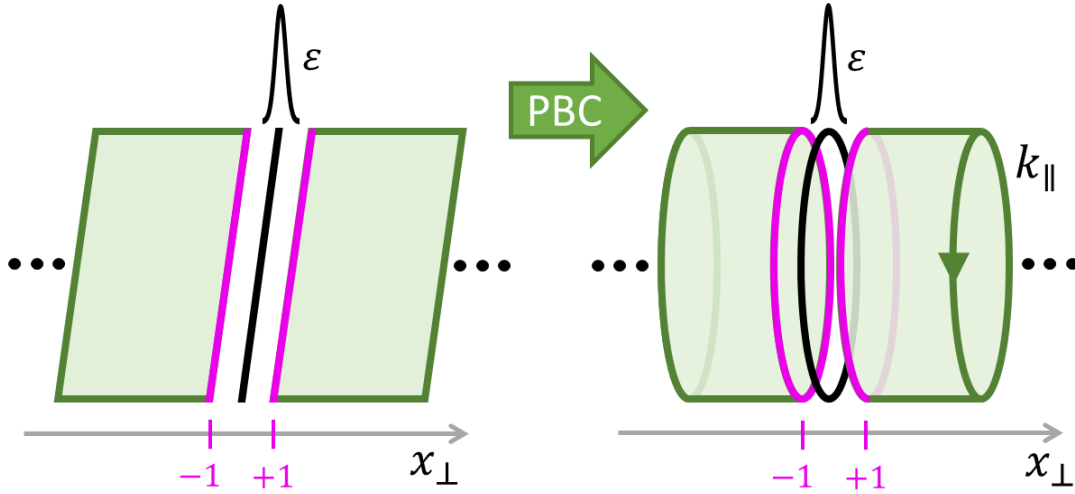


Figure 1: Cylindrical geometry obtained by applying periodic boundary conditions (PBC) along the direction parallel to the boundary in a 2D plane, where x_{\perp} denotes a coordinate in the perpendicular direction measured in units of the lattice constant. In this geometry there is a well defined momentum k_{\parallel} and the open boundaries at $x_{\perp} = \pm 1$ (magenta lines) are obtained by adding a localized impurity line with an amplitude $\varepsilon \rightarrow \infty$ (black line) at $x_{\perp} = 0$. The impurity line breaks the translational symmetry in the x_{\perp} -direction and opens two boundaries in the bulk infinite system.

27 1 Introduction

28 In recent years, due to the appearance of twistrionics [1, 2] and specially since the discovery of
 29 the special properties of twisted bilayer graphene at the magic angle [3, 4], there is a renewed
 30 interest in 2D topological materials exhibiting different phases of matter (e.g. superconductiv-
 31 ity, magnetism, nematicity, etc). In these systems new phenomena arise from the combination
 32 of strong interactions and topology.

33 These circumstances claim for a flexible unified theoretical framework going beyond ide-
 34 alized minimal models to account for interactions, strongly correlated behaviour, spatial inho-
 35 mogeneities or hybrid devices. Several techniques have been developed to describe these new
 36 2D platforms with special emphasis in the topological properties of open boundaries, like exact
 37 Hamiltonian diagonalization of finite systems, wave matching in finite scattering regions [5],
 38 some analytical techniques to derive effective boundary Hamiltonians [6] or the complemen-
 39 tary approaches provided by T -matrix and Green's function formalisms [7–9]. Nevertheless,
 40 methods based in exact diagonalization of microscopic Hamiltonians may require huge compu-
 41 tational capabilities with information on several model parameters and generally, they provide
 42 only numerical results with, in some cases, little or no insight in the underlying physics. For
 43 these reasons theoretical mesoscopic descriptions of intermediate complexity which could give
 44 us access not only to discrete surface modes but also to a well-defined continuum of excitations
 45 are of great interest.

46 In this work we focus in the calculation of the boundary Green's function (bGF) for such
 47 systems, which encodes the local excitation spectrum at an open boundary. Such information is
 48 of special interest in the case of topological phases where the boundary local density of states
 49 (LDOS)s can reveal the presence of edge states or other type of localized excitations, thus
 50 allowing to check out the bulk-boundary correspondence and computing topological invariants
 51 [10, 11].

52 For this purpose we develop a method which allows to compute the bGF at a $d - 1$ bound-

ary starting from a d dimensional infinite bulk. This method complements the approach of Refs. [12–14] for the calculation of bGFs by introducing the Faddeev-LeVerrier algorithm (FLA) [15–19], allowing to consider general d -dimensional systems with an arbitrary number of degrees of freedom and neighbours. This method performs the Fourier transform (FT) needed to compute GFs with local components in the direction perpendicular to the junction to compute the bGF (see Fig. 1) by the analytic continuation of the momenta into the complex plane followed by residue integration. The FLA requires a low computational cost to obtain both the characteristic polynomial and the adjugate matrix of the secular equation $[\omega\hat{\mathbb{1}} - \hat{H}]$ in the same process which are, the main building blocks to solve the FT using the residue integration.

In addition to giving access to the spectral properties at the edges, bGFs allow the calculation of transport properties in heterostructures by means of non-equilibrium Green’s function techniques [12, 20–24]. In addition the Green’s function formalism allows to incorporate in a natural way electron-phonon and/or electron-electron interaction effects for example by means of diagrammatic techniques [25]. Even more, from bGFs it is possible to deduce effective Hamiltonians including all of these effects and obtain their topological properties [26–28].

In comparison with previous works, the semi-analytical approach used in Refs. [12–14] suffers from rigidity in the definition of the GF as it required analytical expressions for the key building blocks of the formalism, such as the characteristic polynomial. A typical symbolic Laplace expansion to evaluate the characteristic polynomial is highly inefficient with potentially enormous memory demand and computational complexity of $O(N!)$ [29] where N is the total Hamiltonian dimension. This constraint imposes an upper-bound limit to the Hilbert space dimension that can be accounted by this method. In contrast, the only analytical entry required for the FLA is the polynomial decomposition of the Hamiltonian in the analytic continuation variable of the momentum perpendicular to the boundary $z = e^{ik_{\perp}L_{\perp}}$.

In the same spirit, the approach of Ref. [30] also uses the residue theorem to obtain the local components of the GF but taking a different path to get its pole. This method computes the poles by solving a generalized eigenvalue problem in contrast with our approach in which we obtain the poles as the roots of the characteristic polynomial. The main advantage of Ref. [30] approach is the possibility to work in the zero-limit for the broadening term, η , that enters as an imaginary part of the energy and the increased robustness of the code which circumvents the problem of obtaining the characteristic polynomial. In contrast, the residue integration of this approach must be modified by adding extra terms depending on the existence or not of boundary modes, and consequently, its mandatory to use a different routine to determine the existence or not of these localized modes.

Even though our approach is less robust and requires $\eta \neq 0$, it is quite transparent, flexible and easy to implement with a straightforward integration routine independent of the peculiarities of the system. Furthermore our approach exhibits better convergence performance compared to recursive approaches [31–34] for which precision is linked to the number of iterations [14].

The rest of the paper is organized as follows: in Sec. 2, we describe the computation of the Green’s function formalism taking advantage of the residue theorem introduced in Refs. [14, 35]. We then use Dyson’s equation to open a boundary in the bulk system with an infinity impurity perturbation. Sec. 3, we describe our method based on FLA to compute the boundary Green’s functions with barely no analytical demands to operate. In Sec. 4, we use some relevant model Hamiltonians for 2D topological systems as examples to compute steadily the FLA, first in a purely analytic problem to then jump into purely computational approaches. These models include the 2D Chern insulator [36], the 2D Kitaev topological superconductor [37] and the Checkerboard lattice hosting topological flat bands [38]. Furthermore, we study the spectral properties at edges of such 2D models exhibiting topological features like

103 chiral edge states. Sec. 5 includes a study of the convergence of the spectral density of the
 104 semi-infinite translational invariant Checkerboard lattice model comparing the recursive GF
 105 technique with the bGF obtained via FLA.

106 We finally summarize the main results with some conclusions in Sec. 6. Technical details
 107 like the finite system diagonalization or an explicit FLA pseudocode are included in the ap-
 108 pendices. Throughout, we use units with nn hopping amplitude $t = 1$ and lattice parameter
 109 $a = 1$.

110 2 bGF method for 2D lattice models

111 To obtain the bGF we start from a d -dimensional bulk infinite system and introduce local
 112 perturbations with the characteristic profile that defines the boundary. As these local pertur-
 113 bations or impurity surface amplitude tends to infinity we are left with two $(d-1)$ -dimensional
 114 open surfaces [7, 8] e.g. two boundary lines in a 2D system induced by an impurity line, see
 115 Fig. 1. The bGF is obtained using the Dyson equations associated to the local surface impurity
 116 potential which breaks translational symmetry albeit the momenta in the direction parallel to
 117 the impurity surface are conserved and thus well defined.

118 The starting GF must be explicitly dependent on the local coordinate associated to the
 119 perpendicular direction to the boundary. In order to get these real space GFs, starting from
 120 $N \times N$ tight-binding Hamiltonians in momentum space $\hat{\mathcal{H}}(\mathbf{k})$, we have to compute the FT of the
 121 bulk GF in the direction perpendicular to the boundary. For this purpose, we decompose the
 122 momenta into parallel and perpendicular components $\mathbf{k} = (k_{\parallel}, k_{\perp})$ relative to the boundary
 123 direction (in higher dimensional models the parallel momentum component would be itself
 124 a vector \mathbf{k}_{\parallel}). The bulk Hamiltonian periodicity in both directions is set by $(L_{\parallel}, L_{\perp})$, such that
 125 $\hat{\mathcal{H}}(\mathbf{k} + 2\pi\mathbf{u}_{\perp}/L_{\perp}) = \hat{\mathcal{H}}(\mathbf{k})$, where \mathbf{u}_{\perp} is the unitary vector in the perpendicular direction. As
 126 to compute the FT we need orthogonal lattice vectors, in some cases like the triangular lattice
 127 we have to double the primitive cell. Using this periodicity, the Hamiltonian can be expanded
 128 in a Fourier series, $\hat{\mathcal{H}}(\mathbf{k}) = \sum_n \hat{\mathcal{V}}_n(k_{\parallel}) e^{ink_{\perp}L_{\perp}}$, where n covers the number of neighbours, and
 129 Hermiticity implies $\hat{\mathcal{V}}_{-n} = \hat{\mathcal{V}}_n^{\dagger}$. Then, the advanced bulk GF is defined as

$$\hat{G}^A(\mathbf{k}, \omega) = [(\omega - i\eta)\hat{\mathbb{1}} - \hat{\mathcal{H}}(\mathbf{k})]^{-1}, \quad (1)$$

130 where η is a small broadening parameter that ensures the convergence of its analytic properties
 131 [39] (e.g. to compute the spectral densities and integrated quantities). This parameter is
 132 specially needed in the case of recursive methods where the spectrum is approximated by a
 133 finite set of poles. In this work we set $\eta = 2\Delta\omega/n_{\omega}$, where $\Delta\omega$ is the energy window that we
 134 are studying and n_{ω} is the number of points that we are computing within that window. The
 135 $N \times N$ matrix structure is indicated by the hat notation.

136 Fourier transforming along the perpendicular direction, the GF components are given by

$$\hat{G}_{jj'}^A(k_{\parallel}, \omega) = \frac{L_{\perp}}{2\pi} \int_{-\pi/L_{\perp}}^{\pi/L_{\perp}} dk_{\perp} e^{i(j-j')k_{\perp}L_{\perp}} \hat{G}^A(k_{\parallel}, k_{\perp}, \omega), \quad (2)$$

137 where j and j' are lattice site indices in the x_{\perp} -direction. By the identification $z = e^{ik_{\perp}L_{\perp}}$, this
 138 integral is converted into a complex contour integral,

$$\hat{G}_{jj'}^A(k_{\parallel}, \omega) = \frac{1}{2\pi i} \oint_{|z|=1} \frac{dz}{z} z^{j-j'} \hat{G}^A(k_{\parallel}, z, \omega). \quad (3)$$

139 Further simplification can be obtained by introducing the roots $z_n(k_{\parallel}, \omega)$ of the character-
140 istic polynomial in the z -complex plane,

$$P(k_{\parallel}, z, \omega) = \det[\omega \hat{\mathbb{1}} - \hat{\mathcal{H}}(k_{\parallel}, z)] = \frac{c_m}{z^m} \prod_{n=1}^{2m} (z - z_n(k_{\parallel}, \omega)), \quad (4)$$

141 where m is the highest order of the characteristic polynomial and c_m is the highest order
142 coefficient. In terms of these roots the contour integral in Eq. (3) can be written as a sum over
143 the residues of all roots inside the unit circle in the complex plane

$$\hat{G}_{jj'}^A(k_{\parallel}, \omega) = \sum'_{|z_n| < 1} \frac{z_n^q \hat{M}(k_{\parallel}, z_n, \omega)}{c_m \prod_{l \neq n} (z_n - z_l)}, \quad (5)$$

144 where $q = j - j' + m - m' - 1$ and $z^{-m'} \hat{M}(k_{\parallel}, z, \omega)$ is the adjugate matrix of $[\omega \hat{\mathbb{1}} - \hat{\mathcal{H}}(k_{\parallel}, z)]$
145 where all the poles at zero were taken out of \hat{M} as a common factor in $z^{-m'}$. Finally, \sum' means
146 that if $q < 0$ then we include $z_n = 0$ as a pole in the sum of residues (e.g., in the non local GF
147 components with $j' > j$). Consequently when $q < -1$ higher order poles at zero appear in the
148 sum of residues. To simplify these situations we can take advantage of the residue theorem to
149 avoid these poles and compute the integral as

$$\hat{G}_{jj'}^A(k_{\parallel}, \omega) = - \sum'_{|z_n| > 1} \frac{z_n^q \hat{M}(k_{\parallel}, z_n, \omega)}{c_m \prod_{l \neq n} (z_n - z_l)}. \quad (6)$$

150 To simplify the notation, we omit the superscript 'A' denoting advanced GFs from now
151 on. Given the real-space components of the bulk GF in Eq. (5), we next extend the method of
152 Refs. [12, 21, 40] to derive the bGF characterizing a *semi-infinite* nearest-neighbour 2D systems.
153 To this effect, we add an impurity potential line ε localized at the frontier region. Taking the
154 limit $\varepsilon \rightarrow \infty$ the infinite system is cut into two disconnected semi-infinite subsystems with
155 $j \leq -1$ (left side, L) and $j \geq 1$ (right side, R), see Fig. 1. Using Dyson equation the local GF
156 components of the cut subsystem follow as [12]

$$\hat{G}_{jj} = \hat{G}_{jj}^{(0)} - \hat{G}_{j0}^{(0)} [\hat{G}_{00}^{(0)}]^{-1} \hat{G}_{0j}^{(0)}, \quad (7)$$

157 where $\hat{G}^{(0)}$ are the unperturbed bulk GF and \hat{G} are the semi-infinite perturbed GF. Following
158 Eq. (7), the bGF for the left and right semi-infinite systems are respectively given by

$$\hat{G}_L(k_{\parallel}, \omega) = \hat{G}_{\bar{1}\bar{1}}(k_{\parallel}, \omega), \quad \hat{G}_R(k_{\parallel}, \omega) = \hat{G}_{11}(k_{\parallel}, \omega), \quad (8)$$

159 where the over-line in the local indices in the bGF means negative sites. In order to extend the
160 method to the case of interactions to an arbitrary number of neighbours we need to include
161 as many impurity surfaces as the number of neighbours in order to completely disconnect
162 two semi-infinite regions. In an equivalent fashion we could obtain a new Dyson equation
163 to compute the bGF of the system. Another possibility would be to define a supercell that
164 transforms the Hamiltonian into a nearest-neighbour one with respect to this supercell and
165 compute the bGF applying Eq. (8). Using this bGF we can compute the spectral properties of
166 open (semi-infinite or finite) systems encoded in the spectral densities and the local density of
167 states respectively

$$\rho_{L,R}(k_{\parallel}, \omega) = \frac{1}{\pi} \Im \{ \hat{G}_{L,R}(k_{\parallel}, \omega) \}, \quad \langle \rho_{L,R}(\omega) \rangle = \int \frac{dk_{\parallel}}{\Omega_{k_{\parallel}}} \rho_{L,R}(k_{\parallel}, \omega), \quad (9)$$

168 where $\Omega_{k_{\parallel}} = 2\pi/L_{\parallel}$ accounts for the limits of integration.

169 3 Faddeev-LeVerrier algorithm

170 We first summarize FLA for a generic complex matrix. Let \hat{A} be a $N \times N$ matrix with char-
 171 acteristic polynomial $P(\omega) = \det[\omega\hat{\mathbb{1}} - \hat{A}] = \sum_{k=0}^n \bar{C}_k \omega^k$. The trivial coefficients are $\bar{C}_n = 1$
 172 and $\bar{C}_0 = (-1)^n \det \hat{A}$, also simple is the term $\bar{C}_{n-1} = -\text{tr}\{\hat{A}\}$. The other coefficients can be
 173 calculated using the Faddeev-LeVerrier algorithm [15–19] as

$$\hat{M}_k = \hat{A}\hat{M}_{k-1} + \bar{C}_{n-k+1}\hat{\mathbb{1}}, \quad \bar{C}_{n-k} = -\frac{1}{k}\text{tr}\{\hat{A}\hat{M}_k\}, \quad (10)$$

174 where \hat{M}_k is an auxiliary matrix such that $\hat{M}_0 = 0$. Remarkably the matrices \hat{M}_k allow us to
 175 obtain the adjugate matrix of $[\omega\hat{\mathbb{1}} - \hat{A}]$ as a polynomial

$$\text{adj}[\omega\hat{\mathbb{1}} - \hat{A}] = \sum_{k=0}^n \omega^k \hat{M}_{n-k}, \quad (11)$$

176 which, given that $\hat{M}_0 = \hat{0}$, the adjugate matrix $\hat{M}(\omega)$ has $N - 1$ order in ω .

177 In our case $\hat{A} \equiv \hat{\mathcal{H}}(z)$ is a polynomial complex matrix and it can also be expanded as a
 178 polynomial in z as

$$\hat{\mathcal{H}}(z) = \sum_{i=1}^{2m+1} \hat{H}_i z^{i-(m+1)} = \hat{H}_1 z^{-m} + \dots + \hat{H}_{m+1} + \dots + \hat{H}_{2m+1} z^m. \quad (12)$$

179 In some simple cases where $\text{rg}(\hat{H}_{2m+1}) = N$ we get the highest order polynomial decom-
 180 position for the Hamiltonian and $m = n_n N$ where n_n is equal to the number of neighbours in
 181 the tight-binding model, but in general $m \leq n_n N$.

182 We are interested in expressing \bar{C}_k and \hat{M}_k as two-variable polynomials in ω and z using
 183 two variable FLA [41–43] to compute the complex integral. Still we have $\bar{C}_n = 1$ and $\hat{M}_1 = \hat{\mathbb{1}}$.
 184 Then,

$$\bar{C}_{n-1}(z) = -\text{tr}\{\hat{\mathcal{H}}(z)\} = \sum_{i=1}^{2m+1} \bar{C}_{n-1,i} z^{i-(m+1)}. \quad (13)$$

185 For example, the next coefficients are

$$\hat{M}_2(z) = \hat{\mathcal{H}}(z) + \bar{C}_{n-1} \hat{\mathbb{1}} = \sum_{i=1}^{2m+1} \hat{M}_{2,i} z^{i-(m+1)}, \quad \bar{C}_{n-2}(z) = -\frac{1}{2}\text{tr}\{\hat{\mathcal{H}}(z)\hat{M}_2(z)\} = \sum_{i=1}^{4m+1} \bar{C}_{n-2,i} z^{i-(2m+1)}. \quad (14)$$

186 In this way we could get

$$\hat{M}_k(z) = \sum_{i=1}^{2m(k-1)+1} \hat{M}_{k,i} z^{i-(m(k-1)+1)}, \quad \bar{C}_{n-k}(z) = \sum_{i=i}^{2mk+1} \bar{C}_{n-k,i} z^{i-(mk+1)}, \quad (15)$$

187 and deduce an explicit decomposition of $\text{adj}[\omega\hat{\mathbb{1}} - \hat{\mathcal{H}}(k_{\parallel}, z)]$ in z from which we can extract
 188 the zero poles of the adjugate matrix $z^{-m'}$ as in Eq. (5). In simple cases where $m = n_n N$, it is
 189 straightforward to see that $m' = N - 1$.

190 In Fig. 2 we expose the general structure of the complete algorithm to compute the bGF
 191 given, as an input, the polynomial decomposition of the Hamiltonian particularized at any
 192 k_{\parallel} . Using FLA we obtain the auxiliary matrix to compute the adjugate of the secular equation
 193 $\hat{M}(k_{\parallel})$ and the coefficients of the characteristic polynomial $\bar{C}(k_{\parallel})$, see Appendix B. From $\bar{C}(k_{\parallel})$
 194 we can compute the characteristic polynomial $P(k_{\parallel}, \omega)$ for any desired frequency and solve it
 195 to obtain the roots $z_n(k_{\parallel}, \omega)$.

bGF COMPUTATION

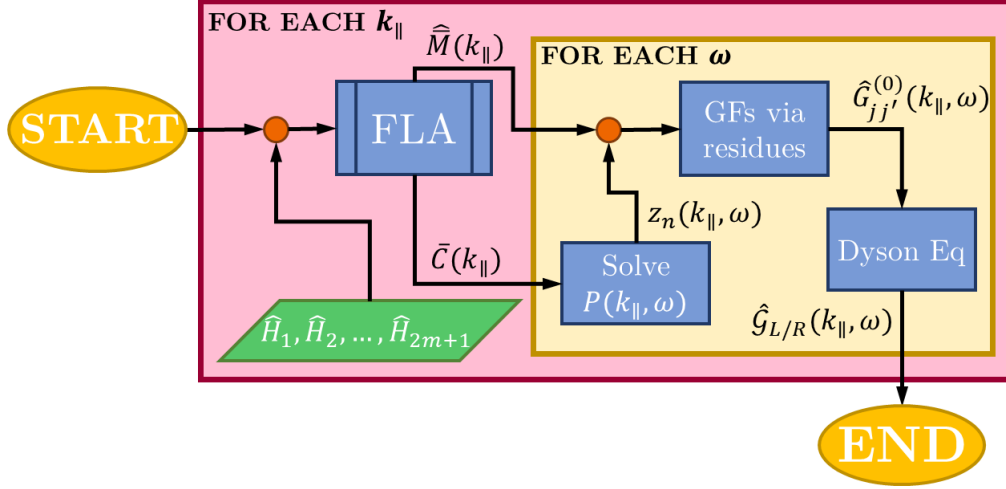


Figure 2: Complete algorithm workflow to compute the bGF using the FLA where the main input is the polynomial decomposition of the Hamiltonian for a given set of momenta k_{\parallel} and frequencies ω .

196 Both $z_n(k_{\parallel}, \omega)$ and $\hat{M}(k_{\parallel})$ are the key ingredients to compute the unperturbed GFs in real
 197 space using Eq. (6) and taking as poles the roots that satisfy that $|z_n(k_{\parallel}, \omega)| > 1$. The order of
 198 the zero poles m and m' are totally determined by the polynomial decomposition in z of $\tilde{C}(k_{\parallel})$
 199 and $\hat{M}(k_{\parallel})$ respectively. Finally, we use Dyson equation to compute the bGFs of the system
 200 from the unperturbed ones.

201 4 Tight-binding models

202 In order to illustrate our method in a transparent self-explanatory way we take the example
 203 of common, well-known 2D topological Hamiltonians to compute the bGF explicitly. First, we
 204 start with the fully analytical 2×2 Chern insulator model [36] hosting chiral edge states to
 205 easily follow the FLA step by step. Later we consider more intricate examples where we have
 206 to partially or totally take advantage of the computational power of the FLA. These models
 207 include the 2D Kitaev model [37] for a topological superconductor showing Majorana edge
 208 modes and the 2D Checkerboard model which hosts topological flat bands with chiral edge
 209 states [38]. All these examples are relevant models for the study of topological matter in 2D
 210 and thus we exhibit the spectral density and the LDOS for an open boundary semi-infinite
 211 system to make explicit their topological edge properties. In Fig. 3 a) we show the Brillouin
 212 zone (BZ) for all of these different lattice models.

213 4.1 Chern insulator

214 We first illustrate the FLA with the well-known 2×2 Chern insulator Hamiltonian [36] in a
 215 square lattice described by

$$\hat{H}(\mathbf{k}) = (M - \cos k_y - \cos k_x)\sigma_z + \sin k_x\sigma_x + \sin k_y\sigma_y, \quad (16)$$

216 where σ_{μ} with $\mu = x, y, z$ are the Pauli matrices and M is the mass term.

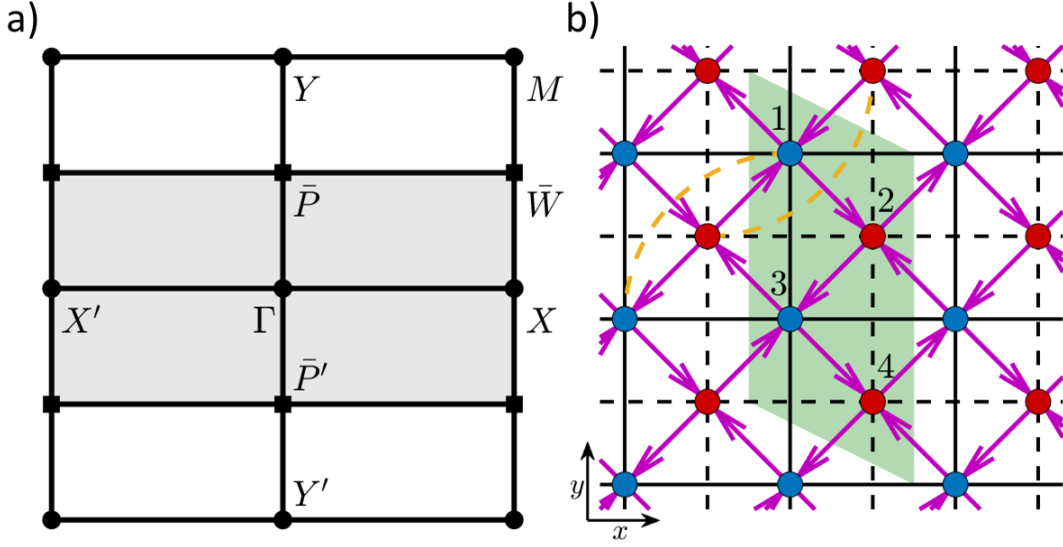


Figure 3: Brillouin zone for the square lattice models and real space representation of the Checkerboard lattice model. a) Square (white) and rectangular (grey shaded) BZ showing the high symmetry points in each one. The over-line in the high symmetry points denotes that they belong to the folded rectangular BZ in the k_y -direction. b) Checkerboard lattice. Red and blue dots indicate the sublattice sites. The magenta arrow, black dashed (solid) line and yellow dashed line accounts for the nn hopping t , the nnn hopping t'_1 (t'_2) and the $nnnn$ hopping t'' respectively. The arrow direction shows the sign of the accumulated phase ϕ in the nn hopping terms. The shaded green region in b) corresponds to the doubling of the original primitive cell which produces the folding of the square BZ into a rectangular one as indicated in panel a).

217 We FT along $k_x = k_\perp$ thereby we made the analytic continuation $z = e^{ik_x}$. We can now
218 obtain the polynomial expansion of the Hamiltonian in z following Eq. (12) where

$$\hat{H}_1 = \hat{H}_3^\dagger = (i\sigma_x - \sigma_z)/2, \quad \hat{H}_2 = (M - \cos k_y)\sigma_z + \sin k_y \sigma_y. \quad (17)$$

219 We then compute the trivial \bar{C}_n coefficients that define the characteristic polynomial in
220 frequencies (ω)

$$\bar{C}_2 = 1, \quad \bar{C}_1 = 0, \quad \bar{C}_0 = (M - \cos k_y)(z + z^{-1}) - [M^2 + 2(1 - M \cos k_y)], \quad (18)$$

221 consequently, their explicit decomposition in the z polynomial

$$\bar{C}_{02} = \bar{C}_{04}^* = (M - \cos k_y), \quad \bar{C}_{03} = -[M^2 + 2(1 - M \cos k_y)]. \quad (19)$$

222 Due to the aforementioned relation, as $\text{rg}(\hat{H}_{2m+1}) < N$, then $m < n_n N$ and for that we
223 have a reduced degree of the characteristic polynomial obeying $\bar{C}_{01} = \bar{C}_{05} = 0$. Nevertheless,
224 we have used the indexation of the polynomial in z as the maximum degree polynomial for
225 the sake of generalization of the method, similarly to the criteria taken in the pseudocode
226 formulation in Appendix B.

227 Then, the characteristic polynomial takes the form

$$P(\omega) = (M - \cos k_y)(z + z^{-1}) + \omega^2 - M^2 - 2(1 - M \cos k_y), \quad (20)$$

228 where $c_m = \bar{C}_{04}$ and the non-trivial contributions to \hat{M} matrix are defined by

$$\hat{M}_{21} = \hat{H}_1 + c_{11}\hat{\mathbb{I}} = \hat{H}_1, \quad \hat{M}_{22} = \hat{H}_2 + c_{12}\hat{\mathbb{I}} = \hat{H}_2, \quad \hat{M}_{23} = \hat{H}_3 + c_{13}\hat{\mathbb{I}} = \hat{H}_3. \quad (21)$$

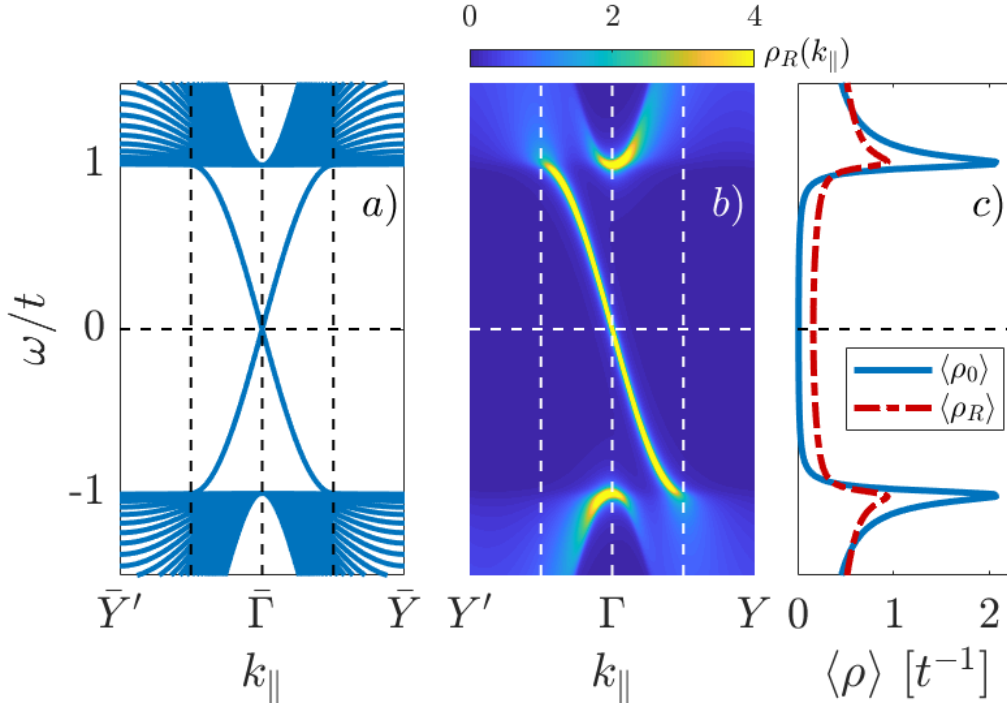


Figure 4: Open boundary characterization for the Chern Insulator model showing chiral edge states under the effect of the mass term $M \rightarrow 1$. a) Electronic bands obtained by exact diagonalization of a finite size system with $N_{sites} = 40$ sites. The spectrum shows 2 chiral edge states each one associated to a different boundary. b) Spectral density for a right boundary in the semi-infinite limit obtained from the bGF calculation. c) Integrated LDOS where straight (dot-dashed) line represents bulk (right boundary) LDOS.

229 Finally, the integral by residues for the bulk GF takes the form

$$\hat{G}_{jj'}(k_y, \omega) = -\frac{z_-^{j-j'}}{z_-} \frac{\begin{pmatrix} -(1+z_-^2) + \alpha z_- & i(1-z_-^2) - \beta z_- \\ i(1-z_-^2) + \beta z_- & (1+z_-^2) - \alpha z_- \end{pmatrix}}{2(M - \cos k_y)(z_- - z_+)}, \quad (22)$$

230 where $\alpha = 2(M + \omega - \cos k_y)$, $\beta = i2 \sin k_y$ and we have regularized the zeros of the ad-
 231 jugate matrix $\text{adj}[\omega \hat{\mathbb{1}} - \hat{H}(k_{\parallel}, z)]$ with the zeros of $P(\omega)$ knowing that $m = m' = 1$. Fur-
 232 thermore, we solve the trivial roots for $P(\omega)$ in Eq. (20), $z_{\pm} = (-b \pm \sqrt{b^2 - 4})/2$ where
 233 $b = [\omega^2 - M^2 - 2(1 - M \cos k_y)]/(M - \cos k_y)$ defining $|z_-| > 1$ and $|z_+| < 1$. Once the
 234 bulk GF in real space has been constructed we use Eq. (8) to obtain the corresponding bGFs.
 235 In Fig. 4 we illustrate the open boundary spectral density for the topological phase of the Chern
 236 insulator exhibiting chiral edge states obtained using FLA. For comparison we also show the
 237 bands obtained using exact finite size Hamiltonian diagonalization, see Appendix A. As can be
 238 observed, while two chiral edge states are present in the finite system calculation, only one
 239 appears in the bGF calculation as expected for a semi-infinite system.

240 4.2 2D Kitaev square lattice

241 Now we apply FLA to obtain the characteristic polynomial of the 2×2 Kitaev square lattice
 242 model [37] and solve it computationally, in this way we can then obtain the bGF in a semi-

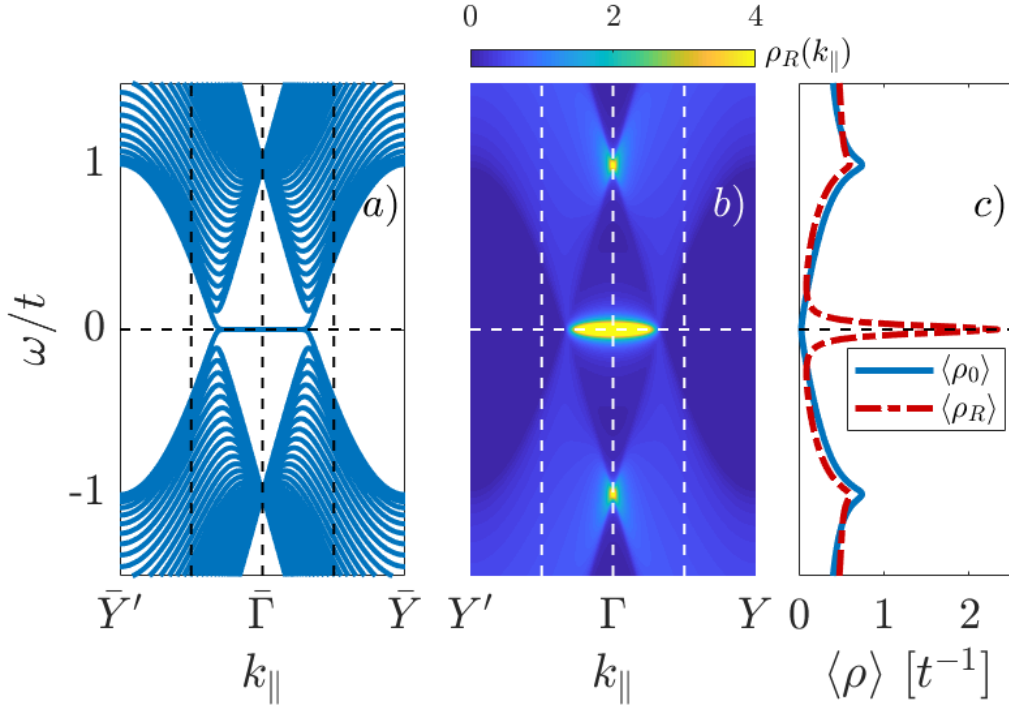


Figure 5: Open boundary characterization for the 2D Kitaev model showing Majorana flat band edge modes in the topological phase $\Delta = 1$ and $\mu = 1$. a) Electronic bands obtained by exact diagonalization of a finite size system with $N_{sites} = 40$ sites. The spectrum shows flat bands at both ends of the system. b) Spectral density for a right boundary in the semi-infinite limit obtained from the bGF calculation. c) Integrated LDOS where straight (dot-dashed) line represents bulk (right boundary) LDOS.

243 analytic manner. The model Hamiltonian is given by

$$\hat{H}(\mathbf{k}) = (\mu - \cos k_y - \cos k_x)\sigma_z - \Delta(\sin k_x + \sin k_y)\sigma_y, \quad (23)$$

244 where μ is the chemical potential and Δ is the pairing potential.

245 Again, the FT along $k_x = k_{\perp}$ is obtained using the analytic continuation $z = e^{ik_x}$. The
246 polynomial expansion of the Hamiltonian in z takes the expression

$$\hat{H}_1 = \hat{H}_3^{\dagger} = (-\sigma_z - i\Delta\sigma_y)/2, \quad \hat{H}_2 = (\mu - \cos k_y)\sigma_z + -\Delta \sin k_y \sigma_y. \quad (24)$$

247 We next compute the \bar{C}_n coefficients that define the characteristic polynomial in powers of
248 ω and z

$$\begin{aligned} \bar{C}_2 = 1, \quad \bar{C}_1 = 0, \quad \bar{C}_{01} = \bar{C}_{05}^* = (\Delta^2 - 1)/4, \quad \bar{C}_{02} = \bar{C}_{04}^* = (\mu - \cos k_y) - i\Delta^2 \sin k_y, \\ \bar{C}_{03} = \frac{(\Delta^2 - 1)}{2} \cos 2k_y + 2\mu \cos k_y - (1 + \Delta^2 + \mu^2), \end{aligned} \quad (25)$$

249 where $c_m = \bar{C}_{05}$ and finally the non-trivial contributions to the \hat{M} matrix are defined as

$$\hat{M}_{21} = \hat{H}_1, \quad \hat{M}_{22} = \hat{H}_2, \quad \hat{M}_{23} = \hat{H}_3. \quad (26)$$

250 We regularize the zeros of the $\text{adj}[\omega\hat{\mathbb{1}} - \hat{H}(k_{\parallel}, z)]$ with the zeros of $P(\omega)$ knowing that
251 $m = 2$ and $m' = 1$. The integral by residues for the bulk GF takes the form

$$\hat{G}_{jj'}(k_y, \omega) = -2z_4^{j-j'} \frac{\begin{pmatrix} -(1+z_4^2) + \alpha z_4 & -\Delta[(1-z_4^2) - \beta z_4] \\ \Delta[(1-z_4^2) - \beta z_4] & (1+z_4^2) - \alpha z_4 \end{pmatrix}}{(\Delta^2 - 1)(z_4 - z_1)(z_4 - z_2)(z_4 - z_3)} + (z_4 \longleftrightarrow z_3), \quad (27)$$

252 where $\alpha = 2(\mu + \omega - \cos k_y)$, $\beta = i2 \sin k_y$ and $|z_4|, |z_3| > 1$, thus $|z_2|, |z_1| < 1$. We omit the
 253 explicit analytical expression of the roots of the characteristic 4th degree polynomial due to
 254 their extension. As mentioned before, for this example it is convenient to obtain the roots com-
 255 putationally. In Fig. 5 we show typical results for the open boundary LDOS in the topological
 256 phase of the 2D Kitaev model showing Majorana flat band edge modes. Again, the comparison
 257 with the finite size diagonalization shows good agreement.

258 4.3 Flat band Checkerboard lattice

259 Finally we consider the 2×2 Checkerboard lattice model [38] which hosts topological flat
 260 bands and is defined by the Hamiltonian

$$\hat{\mathcal{H}}(\mathbf{k}) = \Omega_0(\mathbf{k})\hat{\mathbb{1}} + \Omega_1(\mathbf{k})\sigma_x + \Omega_2(\mathbf{k})\sigma_y + \Omega_3(\mathbf{k})\sigma_z, \quad (28)$$

261 where

$$\begin{aligned} \Omega_0(\mathbf{k}) &= (t'_1 + t'_2)(\cos k_x + \cos k_y) + 4t'' \cos k_x \cos k_y, & \Omega_1(\mathbf{k}) &= 4t \cos \phi \cos \frac{k_x}{2} \cos \frac{k_y}{2}, \\ \Omega_2(\mathbf{k}) &= 4t \sin \phi \sin \frac{k_x}{2} \sin \frac{k_y}{2}, & \Omega_3(\mathbf{k}) &= (t'_1 - t'_2)(\cos k_x - \cos k_y). \end{aligned} \quad (29)$$

262 The system is thus characterized by nn hopping t , nnn hopping t'_1, t'_2 and $nnnn$ hopping
 263 t'' terms, also the nn terms accumulate a phase ϕ pointed out in Fig. 3 b).

264 This model is an exemplification of a typical obstacle to tackle with our algorithm due to the
 265 sublattice degree of freedom. Due to that, the Hamiltonian includes lattice spacing fractions,
 266 hence if we try to FT with the analytic continuation $z = e^{ik_\perp L_\perp/2}$ instead of having a complex
 267 integral over the closed unit circle we arrive to an open arc integral in the complex plane, so
 268 we cannot apply the residue theorem to solve it. This kind of problems may also appear in
 269 Bravais lattices with non-orthogonal lattice vectors (e.g. the triangular lattice).

270 To circumvent this kind of obstacles we proceed to double the unit cell to obtain a new
 271 lattice with orthogonal lattice vectors and integer powers of $z = e^{ik_\perp L_\perp}$. The drawbacks of
 272 doubling the unit cell are that we are now working in a folded BZ and we have doubled the
 273 Hamiltonian degrees of freedom. Consequently the Hamiltonian in the new unit cell expressed
 274 in the basis $\Psi_{\mathbf{k}} = (\psi_{A1,\mathbf{k}}, \psi_{B2,\mathbf{k}}, \psi_{A3,\mathbf{k}}, \psi_{B4,\mathbf{k}})^T$ takes the form

$$\hat{\mathcal{H}}(\mathbf{k}) = \begin{pmatrix} \hat{A} & \hat{B} \\ \hat{B}^\dagger & \hat{A} \end{pmatrix}, \quad (30)$$

275 with

$$\hat{A} = \begin{pmatrix} \delta_2 & \beta_- \\ \beta_-^* & \delta_1 \end{pmatrix}, \quad \hat{B} = \begin{pmatrix} \alpha_1(1 + e^{ik_y}) & e^{ik_y} \beta_+^* \\ \beta_+ & \alpha_2(1 + e^{ik_y}) \end{pmatrix}, \quad (31)$$

276 where $\beta_\pm = e^{\pm i(k_x \pm \phi)} + e^{-i\phi}$, $\alpha_\mu = (t'_\mu + 2t'' \cos k_x)$ and $\delta_\mu = 2t'_\mu \cos k_x$ with $\mu = 1, 2$.

277 In Fig. 3 b) we show the unit cell doubling in the y -direction for the Checkerboard lattice
 278 problem leading to a folded BZ along the k_y -direction. To avoid foldings in the spectral
 279 densities we have made the analytic continuation in $z = e^{ik_y}$ with $k_y = k_\perp$, in this way we
 280 have the explicit momenta dependence of the Hamiltonian in the unfolded BZ coordinate
 281 $k_x = k_\parallel$. The polynomial expansion of the Hamiltonian in z adopts the expression

$$\hat{H}_1 = \hat{H}_3^\dagger = \begin{pmatrix} 0 & 0 & 0 & 0 \\ 0 & 0 & 0 & 0 \\ \alpha_1 & 0 & 0 & 0 \\ \beta_+ & \alpha_2 & 0 & 0 \end{pmatrix}, \quad \hat{H}_2 = \begin{pmatrix} \delta_2 & \beta_- & \alpha_1 & 0 \\ \beta_-^* & \delta_1 & \beta_+ & \alpha_2 \\ \alpha_1 & \beta_+^* & \delta_2 & \beta_- \\ 0 & \alpha_2 & \beta_-^* & \delta_1 \end{pmatrix}. \quad (32)$$

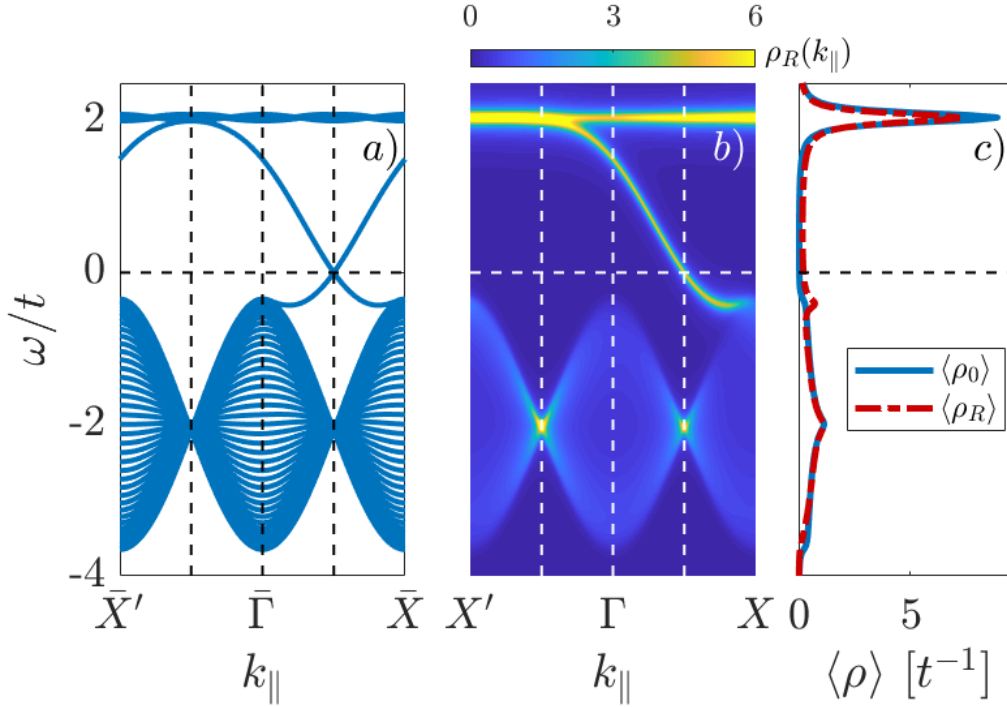


Figure 6: Open boundary characterization for the Checkerboard lattice model showing topological flat band at $\omega/t = 2$ with a chiral edge mode in the topological phase $\phi = -\pi/4$, $t'_1 = -t'_2 = t/(2 + \sqrt{2})$ and $t'' = -t/(2 + 2\sqrt{2})$. a) Electronic bands obtained by exact diagonalization of a finite size system with $N_{sites} = 20$ sites with the unit cell doubled. The spectrum shows 2 chiral edge states each one associated to a different boundary. b) Spectral density for a right boundary in the semi-infinite limit obtained from the bGF calculation. c) Integrated LDOS where straight (dot-dashed) line represents bulk (right boundary) LDOS.

282 Due to the cell doubling we have a characteristic off-diagonal representation of the z dependent terms of the Hamiltonian which induces that $\text{rg}(\hat{H}_{2m+1}) < N$, then again we have a degree reduction of the characteristic polynomial. We now could obtain analytically the \bar{C}_n coefficients that define the characteristic polynomial but we omitted them due to their extension. 284
 285 These coefficients along with the adjugate matrix $\hat{M}(k_{\parallel}, z, \omega)$ can be obtained computationally 286
 287 in a straightforward way using Eq. (14), see Appendix B.

288 In Fig. 6 we show results for the open boundary LDOS for the topological phase of the 289
 289 Checkerboard lattice model exhibiting topological flat bands and chiral edge states. Again, 290
 290 the comparison with the bands obtained by direct diagonalization gives excellent agreement, 291
 291 except for the doubling of the edge states.

292 5 Comparison with recursive approaches

293 As mentioned before, the recursive GF method is a well established tool to compute bGFs. 294
 294 Below we briefly describe the recursive method taking advantage of the Hamiltonian decomposition 295
 295 into two perpendicular directions already introduced for FLA. We define the recursive 296
 296 method to compute the bGF at a dimensionless n -site as

$$[\hat{G}_R^{rc}(n)]^{-1} = \omega \hat{1} - \hat{H}_0(k_{\parallel}) - \Sigma_R(n), \quad [\hat{G}_L^{rc}(n)]^{-1} = \omega \hat{1} - \hat{H}_0(k_{\parallel}) - \Sigma_L(n), \quad (33)$$

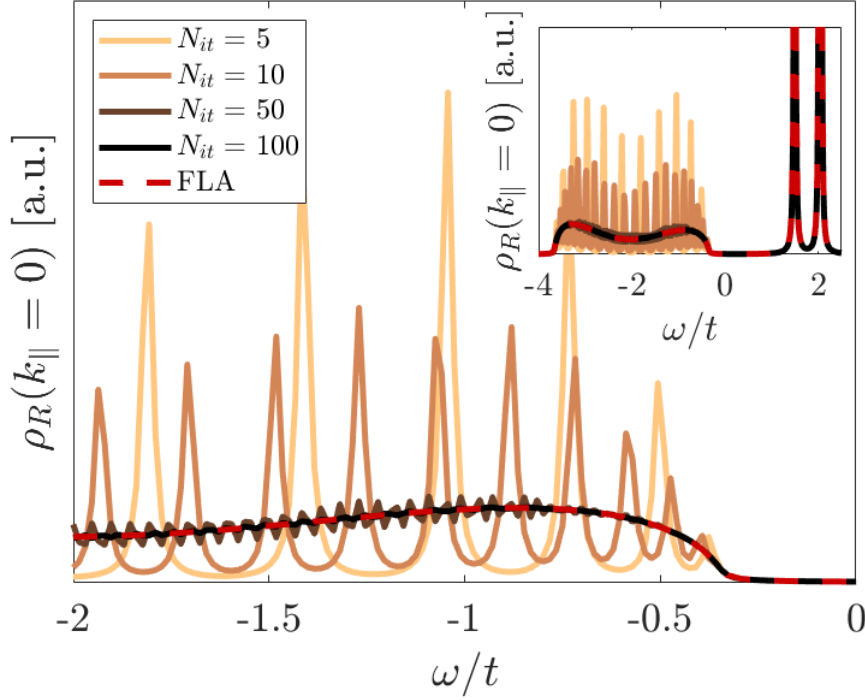


Figure 7: Open right boundary spectral density at $k_{\parallel} = \Gamma$ for the Checkerboard lattice model with $\eta = 0.02$ and the rest of parameters are the same as in Fig. 6. Solid lines represents the spectral density obtained by recursive GF for different number of recursive steps $N_{it} = 5, 10, 50$. Dashed red line is obtained using FLA. Main figure: top continuum valence bands contribution to the spectral density showing the discretization effect of the recursive method. Inset: All the contributions to the spectral density including the flat band at $\omega/t = 2$ and the topological chiral edge state at $\omega/t \approx 1.5$

297 where $\hat{\mathcal{H}}_0(k_{\parallel})$ is the local contribution defined in each iteration step and the recursive expres-
 298 sion of the self-energy takes the form

$$\Sigma_R(n) = \hat{T}_{LR} [\hat{\mathcal{G}}_R^{rc}(n-1)]^{-1} \hat{T}_{LR}^{\dagger}, \quad \Sigma_L(n) = \hat{T}_{LR}^{\dagger} [\hat{\mathcal{G}}_L^{rc}(n-1)]^{-1} \hat{T}_{LR}. \quad (34)$$

299 As can be observed, the self-energy at a given n -site couples this site with the previous one
 300 where n goes from $n = 1$ to $n = N_{it}$ with N_{it} is the number of recursive steps. The self-energy
 301 at the first site $\Sigma_{L/R}(n = 1)$ can be defined to simulate the coupling to a doped continuum of
 302 the same material for better convergence.

303 From the polynomial decomposition of the Hamiltonian in Eq. (12) we can define the
 304 relevant matrices for the recursive method as

$$\hat{\mathcal{H}}_0 = \begin{pmatrix} \hat{H}_{m+1} & \hat{H}_m & \hat{H}_{m-1} & \cdots & \hat{H}_2 \\ \hat{H}_m^{\dagger} & \hat{H}_{m+1} & \hat{H}_m & \cdots & \hat{H}_3 \\ \hat{H}_{m-1}^{\dagger} & \hat{H}_m^{\dagger} & \hat{H}_{m+1} & \cdots & \hat{H}_4 \\ \vdots & \vdots & \vdots & \ddots & \vdots \\ \hat{H}_2^{\dagger} & \hat{H}_3^{\dagger} & \hat{H}_4^{\dagger} & \cdots & \hat{H}_{m+1} \end{pmatrix}, \quad \hat{T}_{LR} = \begin{pmatrix} \hat{H}_1^{\dagger} & \hat{H}_2^{\dagger} & \hat{H}_3^{\dagger} & \cdots & \hat{H}_m^{\dagger} \\ \hat{0} & \hat{H}_1^{\dagger} & \hat{H}_2^{\dagger} & \cdots & \hat{H}_{m-1}^{\dagger} \\ \hat{0} & \hat{0} & \hat{H}_1^{\dagger} & \cdots & \hat{H}_{m-2}^{\dagger} \\ \vdots & \vdots & \vdots & \ddots & \vdots \\ \hat{0} & \hat{0} & \hat{0} & \cdots & \hat{H}_1^{\dagger} \end{pmatrix}. \quad (35)$$

305 Notice that the dimension of the recursive method goes as $N_r = Nn_n$ so for the usual nn
 306 case satisfies $N_r = N$ and $\hat{\mathcal{H}}_0 = \hat{H}_2$, $\hat{T}_{LR} = \hat{H}_1^{\dagger}$.

307 In Fig. 7 we illustrate the convergence of the continuum spectrum within the recursive GF
 308 method for the Checkerboard model at $k_{\parallel} = \Gamma$ with parameters as in Fig. 6 for several number
 309 of iterations compared to bGF obtained using FLA. While the recursive approach accounts well
 310 for discrete states, as boundary states, with few iterations, the number of recursive steps have
 311 to be greatly increased to properly converge the continuum spectrum into the semi-infinite
 312 limit [39]. In contrast, FLA provides an accurate description of both surface modes and con-
 313 tinuum spectra without further computational effort. It is worth mentioning that the recursive
 314 method for all the lattice models in this publication takes from twice to four times more com-
 315 puting time than FLA for the same number of points in the spectral density and $N_{it} = 100$,
 316 for which, as shown in Fig. 7, the recursive calculation has not yet converged to a smooth
 317 continuum spectrum.

318 In order to compare the computational complexity of our technique one should have in
 319 mind that our method could be implemented in a partially analytical way, in the sense that
 320 we can provide an analytical expression for the characteristic polynomial for each of the cases
 321 that we study. The computational complexity is then limited to the evaluation of the roots
 322 of this polynomial which scales roughly as $O(M^2 \log M)$, where $M = 2m$ is the degree of the
 323 polynomial and the maximum degree possible is $M = 2m = 2n_n N$ (e.g., in a typical TB model
 324 up to nn , $M = 2N$ and for that its complexity goes as $\sim O(8N^2 \log N)$). On the contrary, the
 325 well-established recursive GF technique has $O(N_r^3 N_{it})$ complexity [39, 44], where N_{it} typically
 326 $\gg 1$ is the number of iterations required for convergence in a desired energy precision η and
 327 the term N_r^3 is due to matrix inversions where the recursive matrix dimension $N_r = N n_n$ grows
 328 with the number of neighbours.

329 For larger matrix dimensions or higher degree polynomials that the ones analyzed in this
 330 paper, FLA might suffer from numerical instability in the computation of the polynomial co-
 331 efficients due to accumulated errors in the trace in Eq. (10) and from the recursive nature of
 332 the successive polynomial coefficients [45, 46]. However in Ref. [35] FLA was used to obtain
 333 the bGF of TB Hamiltonians that cannot be solved using symbolic approaches due to matrix
 334 dimension (e.g., $N = 12$ Hilbert space dimension). So, despite the potential instability of the
 335 method, it still can be used to efficiently solve the bGF problem of TB Hamiltonians beyond
 336 analytical approaches, at least for moderate dimensions.

337 6 Conclusions and outlook

338 In this work we have extended the boundary Green function method developed in Refs. [14, 35]
 339 to 2D lattices with hopping elements between arbitrary distant neighbors and solved the semi-
 340 analytical obstructions to compute the bGF for large systems, non-orthogonal lattice vectors
 341 or Hamiltonians with terms with momentum fractions. This was made by implementing the
 342 Faddeev-LeVerrier algorithm to compute the characteristic polynomial and the adjugate matrix,
 343 the building blocks to compute the bGF. As an illustration of the method we have analyzed
 344 the spectral properties of different topological 2D Hamiltonians showing the appearance of
 345 topological states.

346 With FLA we can compute the bGF for any TB model with a well-known algorithm and
 347 a simple implementation which provides the coefficients of the characteristic polynomial but
 348 also the adjugate matrix in the same process. Furthermore, FLA can be extended to obtain the
 349 generalized inverses of multiple-variable polynomials or particularly, two-variable polynomials
 350 [41–43].

351 In Ref. [47, 48] it is claimed that the classical Faddeev-LeVerrier algorithm for polynomial
 352 matrices in one variable has $O(N^3 N)$ computational complexity and it avoids any division by
 353 a matrix entry, which it is desirable from the convergence perspective in contrast to recursive

354 approaches. Although the classical FLA is not the most efficient algorithm from the point of
 355 view of complexity (e.g. Berkowitz algorithm [49] is faster), it is a rather simple and general
 356 way to solve the inverse of a polynomial matrix problem. Despite the recursive nature of FLA,
 357 it can be easily modified to carry out the N matrix multiplications in parallel [46, 47, 50, 51].

358 As an outlook, the FLA method can be combined with interpolation approaches [48, 52, 53]
 359 to improve the stability of the algorithm when computing the bGF of TB systems with a large
 360 number of degrees of freedom and neighbours. Furthermore, this method and the recursive
 361 methods could be combined to describe systems with regions with broken translational sym-
 362 metry like two semi-infinite translational invariant regions coupled by a disordered region. In
 363 addition, we foresee the application of the method to study higher order topological insula-
 364 tors [54] which requires projection onto the intersection of two or more edge surfaces.

365 Acknowledgments

366 We acknowledge and thank P. Buset for useful comments on this manuscript. This project has
 367 been funded by the Spanish AEI through Grant No. PID2020-117671GB-I00 and through the
 368 “María de Maeztu” Programme for Units of Excellence in R&D (CEX2018-000805-M).

369 A Exact Hamiltonian diagonalization

370 From the matrices that define the recursive method in Eq. (35) we can also describe the total
 371 Hamiltonian for a finite system to compute an exact diagonalization and obtain the edge state
 372 spectrum.

$$\hat{H}_{TOT} = \begin{pmatrix} \hat{\mathcal{H}}_0 & \hat{T}_{LR} & \hat{0} & \cdots & \hat{0} \\ \hat{T}_{LR}^\dagger & \hat{\mathcal{H}}_0 & \hat{T}_{LR} & \cdots & \hat{0} \\ \hat{0} & \hat{T}_{LR}^\dagger & \hat{\mathcal{H}}_0 & \cdots & \hat{0} \\ \vdots & \vdots & \vdots & \ddots & \vdots \\ \hat{0} & \hat{0} & \hat{0} & \cdots & \hat{\mathcal{H}}_0 \end{pmatrix}, \quad (36)$$

373 where the main diagonal has N_{sites} block elements and total dimension $N_d = N_{sites}Nn_n$ so for
 374 the usual nn case satisfies $N_d = N_{sites}N$ and $\hat{\mathcal{H}}_0 = \hat{H}_2$, $\hat{T}_{LR} = \hat{H}_1^\dagger$.

375 B Faddeev-LeVerrier algorithm

376 We include here a simple pseudocode description of the classic FLA [15–19] to obtain the
 377 coefficients of the characteristic polynomial \bar{C} and the polynomial description of the adjugate
 378 matrix \hat{M} of the secular equation $[\omega\hat{\mathbb{1}} - \hat{H}]$ from a constant matrix (Algorithm 1).

Algorithm 1 Classic Faddeev-LeVerrier algorithm**Input:** $\hat{H} \in \mathbb{C}^{n \times n}$ where $n \geq 2$ **Output:** (\bar{C}, \hat{M})

- 1: $\bar{C}_n = 1, \hat{M}_1 = \hat{H}, k \leftarrow 2$
- 2: $\bar{C}_{n-1} = -\text{tr}\{\hat{H}\}$
- 3: **while** $k \leq n$ **do**
- 4: $\hat{M}_k \leftarrow \hat{H}\hat{M}_{k-1} + \bar{C}_{n-k+1}\hat{H}$
- 5: $\bar{C}_{n-k} \leftarrow -\frac{1}{k}\text{tr}\{\hat{H}\hat{M}_k\}$
- 6: $k \leftarrow k + 1$
- 7: **end while**

379 We also describe the modified FLA for two variable polynomials in (ω, z) where the matrix
 380 itself $\hat{\mathcal{H}}(z)$ is a polynomial matrix [41–43] given as an entry the polynomial decomposition in
 381 z of the Hamiltonian as in Eq. (12) (Algorithm 2).

Algorithm 2 Two-variable Faddeev-LeVerrier algorithm

Input: $\hat{H}_1, \hat{H}_2, \dots, \hat{H}_{2m+1} \in \mathbb{C}^{n \times n}$ where $n \geq 2$

Output: (\bar{C}, \hat{M})

- 1: $\bar{C}_n = 1, \hat{M}_1 = \hat{\mathbb{I}}, k \leftarrow 2$
- 2: $\bar{C}_{n-1,1} = -\text{tr}\{\hat{H}_1\}, \bar{C}_{n-1,2} = -\text{tr}\{\hat{H}_2\}, \dots,$
 $\bar{C}_{n-1,2m+1} = -\text{tr}\{\hat{H}_{2m+1}\}$
- 3: **while** $k \leq n$ **do**
- 4: **for** $i \leftarrow 1 : 2m(k-1) + 1$ **do**
- 5: **if** $i \leq 2m(k-2) + 1$ **then**
- 6: $\hat{M}_{k,i} \leftarrow \hat{M}_{k,i} + \hat{H}_1 \hat{M}_{k-1,i}$
- 7: **end if**
- 8: **if** $i \geq 2$ **and** $i \leq 2m(k-2) + 2$ **then**
- 9: $\hat{M}_{k,i} \leftarrow \hat{M}_{k,i} + \hat{H}_2 \hat{M}_{k-1,i}$
- 10: **end if**
- 11: ...
- 12: **if** $i \geq 2m + 1$ **and** $i \leq 2m(k-2) + 2m + 1$ **then**
- 13: $\hat{M}_{k,i} \leftarrow \hat{M}_{k,i} + \hat{H}_{2m+1} \hat{M}_{k-1,i}$
- 14: **end if**
- 15: $\hat{M}_{k,i} \leftarrow \hat{M}_{k,i} + \bar{C}_{n-k+1} \hat{\mathbb{I}}$
- 16: **end for**
- 17: **for** $i \leftarrow 1 : 2mk + 1$ **do**
- 18: **if** $i \leq 2m(k-1) + 1$ **then**
- 19: $\bar{C}_{n-k,i} \leftarrow \bar{C}_{n-k,i} - \frac{1}{k} \text{tr}\{\hat{H}_1 \hat{M}_{k,1}\}$
- 20: **end if**
- 21: **if** $i \geq 2$ **and** $i \leq 2m(k-1) + 2$ **then**
- 22: $\bar{C}_{n-k,i} \leftarrow \bar{C}_{n-k,i} - \frac{1}{k} \text{tr}\{\hat{H}_2 \hat{M}_{k,i}\}$
- 23: **end if**
- 24: ...
- 25: **if** $i \geq 2m + 1$ **and** $i \leq 2m(k-1) + 2m + 1$ **then**
- 26: $\bar{C}_{n-k,i} \leftarrow \bar{C}_{n-k,i} - \frac{1}{k} \text{tr}\{\hat{H}_{2m+1} \hat{M}_{k,i}\}$
- 27: **end if**
- 28: **end for**
- 29: $k \leftarrow k + 1$
- 30: **end while**

382 **References**

- 383 [1] S. Carr, D. Massatt, S. Fang, P. Cazeaux, M. Luskin and E. Kaxiras, *Twistronics: Manip-*
384 *ulating the electronic properties of two-dimensional layered structures through their twist*
385 *angle*, Phys. Rev. B **95**, 075420 (2017), doi:[10.1103/PhysRevB.95.075420](https://doi.org/10.1103/PhysRevB.95.075420).
- 386 [2] R. Ribeiro-Palau, C. Zhang, K. Watanabe, T. Taniguchi, J. Hone and C. R. Dean, *Twistable*
387 *electronics with dynamically rotatable heterostructures*, Science **361**(6403), 690 (2018),
388 doi:[10.1126/science.aat6981](https://doi.org/10.1126/science.aat6981).
- 389 [3] Y. Cao, V. Fatemi, S. Fang, K. Watanabe, T. Taniguchi, E. Kaxiras and P. Jarillo-Herrero, *Un-*
390 *conventional superconductivity in magic-angle graphene superlattices*, Nature **556**(7699),
391 43 (2018), doi:<https://doi.org/10.1038/nature26160>.

- 392 [4] Y. Cao, V. Fatemi, A. Demir, S. Fang, S. L. Tomarken, J. Y. Luo, J. D. Sanchez-
393 Yamagishi, K. Watanabe, T. Taniguchi, E. Kaxiras *et al.*, *Correlated insulator behaviour*
394 *at half-filling in magic-angle graphene superlattices*, *Nature* **556**(7699), 80 (2018),
395 doi:<https://doi.org/10.1038/nature26154>.
- 396 [5] M. Istas, C. Groth, A. R. Akhmerov, M. Wimmer and X. Waintal, *A general algorithm*
397 *for computing bound states in infinite tight-binding systems*, *SciPost Phys.* **4**, 26 (2018),
398 doi:[10.21468/SciPostPhys.4.5.026](https://doi.org/10.21468/SciPostPhys.4.5.026).
- 399 [6] R. S. K. Mong and V. Shivamoggi, *Edge states and the bulk-boundary correspondence in*
400 *dirac hamiltonians*, *Phys. Rev. B* **83**, 125109 (2011), doi:[10.1103/PhysRevB.83.125109](https://doi.org/10.1103/PhysRevB.83.125109).
- 401 [7] S. Pinon, V. Kaladzhyan and C. Bena, *Surface green's functions and boundary modes using*
402 *impurities: Weyl semimetals and topological insulators*, *Phys. Rev. B* **101**, 115405 (2020),
403 doi:[10.1103/PhysRevB.101.115405](https://doi.org/10.1103/PhysRevB.101.115405).
- 404 [8] S. Pinon, V. Kaladzhyan and C. Bena, *Surface green's functions and quasi-*
405 *particle interference in weyl semimetals*, *Phys. Rev. B* **102**, 165117 (2020),
406 doi:[10.1103/PhysRevB.102.165117](https://doi.org/10.1103/PhysRevB.102.165117).
- 407 [9] V. Kaladzhyan, S. Pinon, F. Joucken, Z. Ge, E. A. Quezada-Lopez, T. Taniguchi, K. Watan-
408 abe, J. Velasco and C. Bena, *Surface states and quasiparticle interference in bernal and*
409 *rhombohedral graphite with and without trigonal warping*, *Phys. Rev. B* **104**, 155418
410 (2021), doi:[10.1103/PhysRevB.104.155418](https://doi.org/10.1103/PhysRevB.104.155418).
- 411 [10] A. M. Essin and V. Gurarie, *Bulk-boundary correspondence of topological insu-*
412 *lators from their respective green's functions*, *Phys. Rev. B* **84**, 125132 (2011),
413 doi:[10.1103/PhysRevB.84.125132](https://doi.org/10.1103/PhysRevB.84.125132).
- 414 [11] Y. Peng, Y. Bao and F. von Oppen, *Boundary green functions of topological insulators and*
415 *superconductors*, *Phys. Rev. B* **95**, 235143 (2017), doi:[10.1103/PhysRevB.95.235143](https://doi.org/10.1103/PhysRevB.95.235143).
- 416 [12] A. Zazunov, R. Egger and A. Levy Yeyati, *Low-energy theory of transport in majorana wire*
417 *junctions*, *Phys. Rev. B* **94**, 014502 (2016), doi:[10.1103/PhysRevB.94.014502](https://doi.org/10.1103/PhysRevB.94.014502).
- 418 [13] A. Zazunov, R. Egger, M. Alvarado and A. L. Yeyati, *Josephson effect in multiterminal topo-*
419 *logical junctions*, *Phys. Rev. B* **96**, 024516 (2017), doi:[10.1103/PhysRevB.96.024516](https://doi.org/10.1103/PhysRevB.96.024516).
- 420 [14] M. Alvarado, A. Iks, A. Zazunov, R. Egger and A. L. Yeyati, *Boundary green's function*
421 *approach for spinful single-channel and multichannel majorana nanowires*, *Phys. Rev. B*
422 **101**, 094511 (2020), doi:[10.1103/PhysRevB.101.094511](https://doi.org/10.1103/PhysRevB.101.094511).
- 423 [15] U. Leverrier, *Sur les variations séculaire des éléments des orbites pour les sept planètes*
424 *principales*, *J. de Math (s 1)*, 5 (1840).
- 425 [16] V. N. Faddeeva, *Computational methods of linear algebra*, Tech. rep. (1959).
- 426 [17] G. Fragulis, B. Mertzios and A. Vardoulakis, *Computation of the inverse of a polynomial*
427 *matrix and evaluation of its laurent expansion*, *international Journal of Control* **53**(2),
428 431 (1991), doi:[10.1080/00207179108953626](https://doi.org/10.1080/00207179108953626).
- 429 [18] F. R. Gantmacher, *The theory of matrices, vol. 1, transl. from russian by ka hirsch*, AMS
430 Chelsea Publ., Providence, RI (1998).
- 431 [19] A. Householder, *The Theory of Matrices in Numerical Analysis*, Dover Books on Mathe-
432 matics. Dover Publications, ISBN 9780486145631 (2013).

- 433 [20] J. C. Cuevas, A. Martín-Rodero and A. L. Yeyati, *Hamiltonian approach to the transport*
434 *properties of superconducting quantum point contacts*, Phys. Rev. B **54**, 7366 (1996),
435 doi:[10.1103/PhysRevB.54.7366](https://doi.org/10.1103/PhysRevB.54.7366).
- 436 [21] P. Burset, A. L. Yeyati and A. Martín-Rodero, *Microscopic theory of the proximity*
437 *effect in superconductor-graphene nanostructures*, Phys. Rev. B **77**, 205425 (2008),
438 doi:[10.1103/PhysRevB.77.205425](https://doi.org/10.1103/PhysRevB.77.205425).
- 439 [22] P. Burset, A. L. Yeyati, L. Brey and H. A. Fertig, *Transport in superlattices on single-layer*
440 *graphene*, Phys. Rev. B **83**, 195434 (2011), doi:[10.1103/PhysRevB.83.195434](https://doi.org/10.1103/PhysRevB.83.195434).
- 441 [23] S. Gómez Páez, C. Martínez, W. J. Herrera, A. Levy Yeyati and P. Burset, *Dirac point for-*
442 *mation revealed by andreev tunneling in superlattice-graphene/superconductor junctions*,
443 Phys. Rev. B **100**, 205429 (2019), doi:[10.1103/PhysRevB.100.205429](https://doi.org/10.1103/PhysRevB.100.205429).
- 444 [24] O. E. Casas, S. Gómez Páez, A. Levy Yeyati, P. Burset and W. J. Herrera, *Subgap states in*
445 *two-dimensional spectroscopy of graphene-based superconducting hybrid junctions*, Phys.
446 Rev. B **99**, 144502 (2019), doi:[10.1103/PhysRevB.99.144502](https://doi.org/10.1103/PhysRevB.99.144502).
- 447 [25] L. de la Vega, A. Martín-Rodero, N. Agraït and A. L. Yeyati, *Universal features*
448 *of electron-phonon interactions in atomic wires*, Phys. Rev. B **73**, 075428 (2006),
449 doi:[10.1103/PhysRevB.73.075428](https://doi.org/10.1103/PhysRevB.73.075428).
- 450 [26] Z. Wang and S.-C. Zhang, *Simplified topological invariants for interacting insulators*, Phys.
451 Rev. X **2**, 031008 (2012), doi:[10.1103/PhysRevX.2.031008](https://doi.org/10.1103/PhysRevX.2.031008).
- 452 [27] M. Iraola, N. Heinsdorf, A. Tiwari, D. Lessnich, T. Mertz, F. Ferrari, M. H. Fischer, S. M.
453 Winter, F. Pollmann, T. Neupert, R. Valentí and M. G. Vergniory, *Towards a topological*
454 *quantum chemistry description of correlated systems: the case of the hubbard diamond*
455 *chain*, arXiv preprint arXiv:2101.04135 (2021), doi:[10.1103/physrevb.104.195125](https://doi.org/10.1103/physrevb.104.195125).
- 456 [28] D. Lessnich, S. M. Winter, M. Iraola, M. G. Vergniory and R. Valentí, *Elementary band*
457 *representations for the single-particle green's function of interacting topological insulators*,
458 Physical Review B **104**(8) (2021), doi:[10.1103/physrevb.104.085116](https://doi.org/10.1103/physrevb.104.085116).
- 459 [29] J. Stoer and R. Bulirsch, *Introduction to numerical analysis*, vol. 12, Springer Science &
460 Business Media (2013).
- 461 [30] M. Istaş, C. Groth and X. Waintal, *Pushing the limit of quantum transport simulations*,
462 Phys. Rev. Research **1**, 033188 (2019), doi:[10.1103/PhysRevResearch.1.033188](https://doi.org/10.1103/PhysRevResearch.1.033188).
- 463 [31] R. Haydock, *The recursive solution of the schrodinger equation*, vol. 35 of *Solid*
464 *State Physics*, pp. 215–294. Academic Press, doi:[https://doi.org/10.1016/S0081-](https://doi.org/10.1016/S0081-1947(08)60505-6)
465 [1947\(08\)60505-6](https://doi.org/10.1016/S0081-1947(08)60505-6) (1980).
- 466 [32] A. MacKinnon, *The calculation of transport properties and density of states of dis-*
467 *ordered solids*, Zeitschrift für Physik B Condensed Matter **59**(4), 385 (1985),
468 doi:<https://doi.org/10.1007/BF01328846>.
- 469 [33] M. P. L. Sancho, J. M. L. Sancho, J. M. L. Sancho and J. Rubio, *Highly convergent schemes*
470 *for the calculation of bulk and surface green functions*, Journal of Physics F: Metal Physics
471 **15**(4), 851 (1985), doi:[10.1088/0305-4608/15/4/009](https://doi.org/10.1088/0305-4608/15/4/009).
- 472 [34] V. Viswanath and G. Müller, *The Recursion Method: Application to Many-Body Dynamics*,
473 vol. 23, Springer Science & Business Media (2008).

- 474 [35] M. Alvarado and A. L. Yeyati, *Transport and spectral properties of magic-angle twisted*
475 *bilayer graphene junctions based on local orbital models*, Phys. Rev. B **104**, 075406 (2021),
476 doi:[10.1103/PhysRevB.104.075406](https://doi.org/10.1103/PhysRevB.104.075406).
- 477 [36] B. A. Bernevig, *Topological Insulators and Topological Superconductors*, Princeton Uni-
478 versity Press, ISBN 9781400846733, doi:[doi:10.1515/9781400846733](https://doi.org/10.1515/9781400846733) (2013).
- 479 [37] K. Zhang, P. Wang and Z. Song, *Majorana flat band edge modes of topologi-*
480 *cal gapless phase in 2d kitaev square lattice*, Scientific reports **9**(1), 1 (2019),
481 doi:<https://doi.org/10.1038/s41598-019-41529-y>.
- 482 [38] K. Sun, Z. Gu, H. Katsura and S. Das Sarma, *Nearly flatbands with nontrivial topology*,
483 Phys. Rev. Lett. **106**, 236803 (2011), doi:[10.1103/PhysRevLett.106.236803](https://doi.org/10.1103/PhysRevLett.106.236803).
- 484 [39] J. Velev and W. Butler, *On the equivalence of different techniques for evaluating the green*
485 *function for a semi-infinite system using a localized basis*, Journal of Physics: Condensed
486 Matter **16**(21), R637 (2004), doi:[10.1088/0953-8984/16/21/r01](https://doi.org/10.1088/0953-8984/16/21/r01).
- 487 [40] L. Arrachea, G. S. Lozano and A. A. Aligia, *Thermal transport in one-dimensional spin*
488 *heterostructures*, Phys. Rev. B **80**, 014425 (2009), doi:[10.1103/PhysRevB.80.014425](https://doi.org/10.1103/PhysRevB.80.014425).
- 489 [41] C. S. Koo and C.-T. Chen, *Faddeeva's algorithm for spatial dynamical equations*, Proceedings
490 of the IEEE **65**(6), 975 (1977), doi:[10.1109/PROC.1977.10594](https://doi.org/10.1109/PROC.1977.10594).
- 491 [42] N. Karampetakis, B. Mertzios and A. Vardoulakis, *Computation of the transfer function*
492 *matrix and its laurent expansion of generalized two-dimensional systems*, International
493 Journal of Control **60**(4), 521 (1994), doi:[10.1080/00207179408921479](https://doi.org/10.1080/00207179408921479).
- 494 [43] N. Karampetakis, *Generalized inverses of two-variable polynomial matrices and*
495 *applications*, Circuits, Systems and Signal Processing **16**(4), 439 (1997),
496 doi:<https://doi.org/10.1007/BF01198061>.
- 497 [44] F. Teichert, A. Zienert, J. Schuster and M. Schreiber, *Improved recursive green's function*
498 *formalism for quasi one-dimensional systems with realistic defects*, Journal of Computa-
499 tional Physics **334**, 607 (2017), doi:<https://doi.org/10.1016/j.jcp.2017.01.024>.
- 500 [45] R. Rehman and I. C. F. Ipsen, *La budde's method for computing characteristic polynomials*,
501 arXiv preprint arXiv:1104.3769 (2011), [1104.3769](https://arxiv.org/abs/1104.3769).
- 502 [46] F. Johansson, *On a fast and nearly division-free algorithm for the characteristic polynomial*,
503 arXiv preprint arXiv:2011.12573 (2020), [2011.12573](https://arxiv.org/abs/2011.12573).
- 504 [47] C. Bär, *The faddeev-leverrier algorithm and the pfaffian*, Linear Algebra and its Applica-
505 tions **630**, 39 (2021), doi:<https://doi.org/10.1016/j.laa.2021.07.023>.
- 506 [48] M. D. Petković and P. S. Stanimirović, *Interpolation algorithm of leverrier-*
507 *faddev type for polynomial matrices*, Numerical Algorithms **42**(3), 345 (2006),
508 doi:<https://doi.org/10.1007/s11075-006-9044-4>.
- 509 [49] S. J. Berkowitz, *On computing the determinant in small parallel time using a*
510 *small number of processors*, Information Processing Letters **18**(3), 147 (1984),
511 doi:[https://doi.org/10.1016/0020-0190\(84\)90018-8](https://doi.org/10.1016/0020-0190(84)90018-8).
- 512 [50] F. Preparata and D. Sarwate, *An improved parallel processor bound in fast matrix inversion*,
513 Information Processing Letters **7**(3), 148 (1978), doi:[https://doi.org/10.1016/0020-0190\(78\)90079-0](https://doi.org/10.1016/0020-0190(78)90079-0).
- 514

- 515 [51] L. Csanky, *Fast parallel matrix inversion algorithms*, In *16th Annual Symposium on Founda-*
516 *tions of Computer Science (sfcs 1975)*, pp. 11–12, doi:[10.1109/SFCS.1975.14](https://doi.org/10.1109/SFCS.1975.14) (1975).
- 517 [52] S. Vologiannidis and N. Karampetakis, *Inverses of multivariable polynomial matrices by*
518 *discrete fourier transforms*, *Multidimensional Systems and Signal Processing* **15**(4), 341
519 (2004), doi:<https://doi.org/10.1023/B:MULT.0000037345.60574.d4>.
- 520 [53] N. Karampetakis and A. Evripidou, *On the computation of the inverse of a two-variable*
521 *polynomial matrix by interpolation*, *Multidimensional Systems and Signal Processing* **23**,
522 97 (2012), doi:[10.1007/s11045-010-0102-7](https://doi.org/10.1007/s11045-010-0102-7).
- 523 [54] F. Schindler, A. M. Cook, M. G. Vergniory, Z. Wang, S. S. Parkin, B. A. Bernevig and
524 T. Neupert, *Higher-order topological insulators*, *Science advances* **4**(6), eaat0346 (2018),
525 doi:[10.1126/sciadv.aat0346](https://doi.org/10.1126/sciadv.aat0346).